

Mind the Gap: Aligning Vision Foundation Models to Image Feature Matching

Yuhan Liu Jingwen Fu Yang Wu Kangyi Wu Pengna Li
 Jiayi Wu Sanping Zhou Jingmin Xin[†]

National Key Laboratory of Human-Machine Hybrid Augmented Intelligence,
 National Engineering Research Center for Visual Information and Applications,
 Institute of Artificial Intelligence and Robotics, Xi'an Jiaotong University

{liuyuhan200095, wuyang_cc, wukangyi747600, sauerfisch}@stu.xjtu.edu.cn, jwfu99@gmail.com
 wujiayi0101@163.com, spzhou@xjtu.edu.cn, jxin@mail.xjtu.edu.cn

Abstract

Leveraging the vision foundation models has emerged as a mainstream paradigm that improves the performance of image feature matching. However, previous works have ignored the **misalignment** when introducing the foundation models into feature matching. The misalignment arises from the discrepancy between the foundation models focusing on single-image understanding and the cross-image understanding requirement of feature matching. Specifically, 1) the embeddings derived from commonly used foundation models exhibit discrepancies with the optimal embeddings required for feature matching; 2) lacking an effective mechanism to leverage the single-image understanding ability into cross-image understanding. A significant consequence of the misalignment is they struggle when addressing multi-instance feature matching problems. To address this, we introduce a simple but effective framework, called IMD (Image feature Matching with a pre-trained Diffusion model) with two parts: 1) Unlike the dominant solutions employing contrastive-learning based foundation models that emphasize global semantics, we integrate the generative-based diffusion models to effectively capture instance-level details. 2) We leverage the prompt mechanism in generative model as a natural tunnel, propose a novel cross-image interaction prompting module to facilitate bidirectional information interaction between image pairs. To more accurately measure the misalignment, we propose a new benchmark called IMIM, which focuses on multi-instance scenarios. Our proposed IMD establishes a new state-of-the-art in commonly evaluated benchmarks, and the superior improvement 12% in IMIM indicates our method efficiently mitigates the misalignment.

[†]Corresponding author.

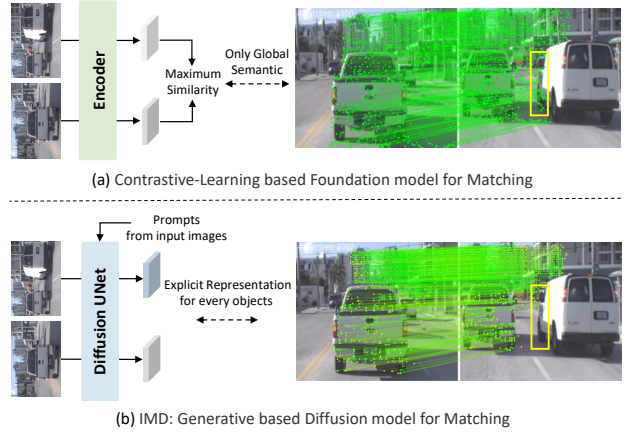


Figure 1. **The main idea of our proposed IMD.** Previous works [15, 28] failed in multi-instance scenarios due to the misalignment. Our IMD leverages the explicit representation of specific instances within the diffusion model with an interaction module, accurately matching the specific instance.

1. Introduction

Image feature matching serves as the foundation for many computer vision tasks, finds extensive applications in areas as image stitching [25, 33], 3D reconstruction [45, 46] and visual localization [6, 41, 43]. Over the past decade, image feature matching has evolved from hand-crafted approaches [4, 39] to learning-based methods [12, 35, 37]. Recently, numerous learnable image matchers [14, 27, 49, 52] trained on real-world datasets [11, 24] have been proposed achieving ever-improving performance. It has been observed that such methods tend to overfit to a specific training distribution or domain and fail to generalize on unseen data fail to generalize on unseen data [21]. Recent approaches [8, 15, 21] have demonstrated that integrating vision foundation models pre-trained on large-scale datasets can effectively solve this issue, achieving superior generalization ability. However, our investigation identifies a non-

negligible misalignment when adapting these vision foundational models to image feature matching.

This misalignment comes from the discrepancy between the vision foundation models focus on understanding the content of the single-image and the cross-image relational understanding requirements for feature matching. The consequence of the misalignment is the poor performance of these methods in multi-instance matching problems as illustrated in Figure 1. In this case, multiple instances of the same object class exist, which impose high requirements on cross-image understanding to locate the correct instance. To address the misalignment issue, this study identifies two critical challenges that need to be confronted:

Challenge I: *Which properties that the foundation model has to equip in order to reduce the misalignment?* Previous works leverage contrastive-learning based foundation model [15, 21, 28], which maximize the similarity between features prioritize global semantics. However, as illustrated in Figure 1(a), these foundation models are sub-optimal for image feature matching, such contrastive objectives often lose information about specific instances and objects [59], which are crucial for accurate matching. To solve this issue, we argue that generative-based foundation models serve as a more suitable alternative. The reason is that the feature of generative-based models contain various objects and instances each with distinctive appearances and structures [40, 51]. As demonstrated in Figure 1(b), this information is crucial for image feature matching, particularly in multiple instances scenarios.

Challenge II: *How to design a cross-image interaction mechanism aligning with the matching tasks?* Although the foundation models have strong single-image understanding ability, they can not lead to cross-image understanding by nature. This paper identifies the condition mechanism of the generative-based model as a natural tunnel for the cross-image information interaction. Inspired by this, we intend to utilize each image as the condition for the other image.

In this paper, we propose **IMD**: Image feature Matching with Diffusion models, seamlessly adapt foundation models to matching tasks. The IMD contains two parts: **1)** We introduce a novel feature extraction paradigm based on the phenomenal generative-based diffusion models, exploring its ability of self-image understanding while moving toward cross-image understanding. Different from previous works utilizing the progressive denoising process [32, 60], we employ the frozen UNet decoder as a backbone to directly process clean natural images to obtain the explicit representation for every instance. **2)** To facilitate interaction between image pairs, we prompt the extraction of diffusion backbone with a novel Cross-image Interaction Prompt Module (CIPM). Specifically, we design a personalized prompt for each image that was conditioned by the image pair to enhance relevance and discriminability. We also propose to

utilize the cross-attention layers to proceed with explicit interaction and comparison between the image pair. CIPM enforces the model to capture the underlying geometric and semantic relationships between images during the feature extraction process itself, resulting in more correlated and comprehensive image features.

For a more comprehensive analysis, we construct a new benchmark IMIM based on a recently published video tracking and segmentation dataset [1]. We observe that existing benchmarks predominantly comprise images containing either a single, prominent object, enabling semantic-based approaches to attain high performance. In contrast, our IMIM contains images with multiple instances of the same semantic (e.g., two cars running), which imposes more stringent requirements for preserving instance-level details. We report a significant improvement of 12% in matching accuracy, demonstrating that our method successfully alleviates the misalignment.

To summarize, we make the following contributions:

- We identify the misalignment when introducing the foundation models into the feature matching tasks with two challenges for solving the misalignment.
- We propose IMD to achieve seamless alignment with 1) a novel feature extraction pipeline for matching tasks and 2) cross-image interaction prompt module towards cross-image understanding.
- IMD is demonstrated to achieve state-of-the-art results across a wide range of benchmarks. What’s more, a new dataset is introduced to evaluate the performance of models in the multi-instance situation.

2. Related Work

Local Feature Matching. Feature matching methods can be broadly classified into three categories: sparse, semi-dense, and dense. Traditional sparse feature matching has been tackled through keypoint detection and description, followed by matching the descriptors [3, 5, 12, 30, 39, 42]. More recently, the semi-dense approach [9, 28, 49, 52] has emerged, also known as detector-free methods, replacing keypoint detection with dense matching at a coarse scale, followed by mutual nearest neighbor extraction and subsequent refinement. The dense approach [14, 15, 63] focuses on estimating a dense warp, aiming to identify every potential pixel-level correspondence. However, they are typically much slower than sparse and semi-dense approaches.

Vision Foundation Models for Matching. There exist prior works leveraging the vision foundation models to improve matching performance. MESA [61] introduced the use of SAM [22] for area matching, narrowing the search space. Nevertheless, the coarse-grained utilization fails to fully leverage the knowledge of foundation models. Another series of works [8, 15, 21, 28] employ vision foun-

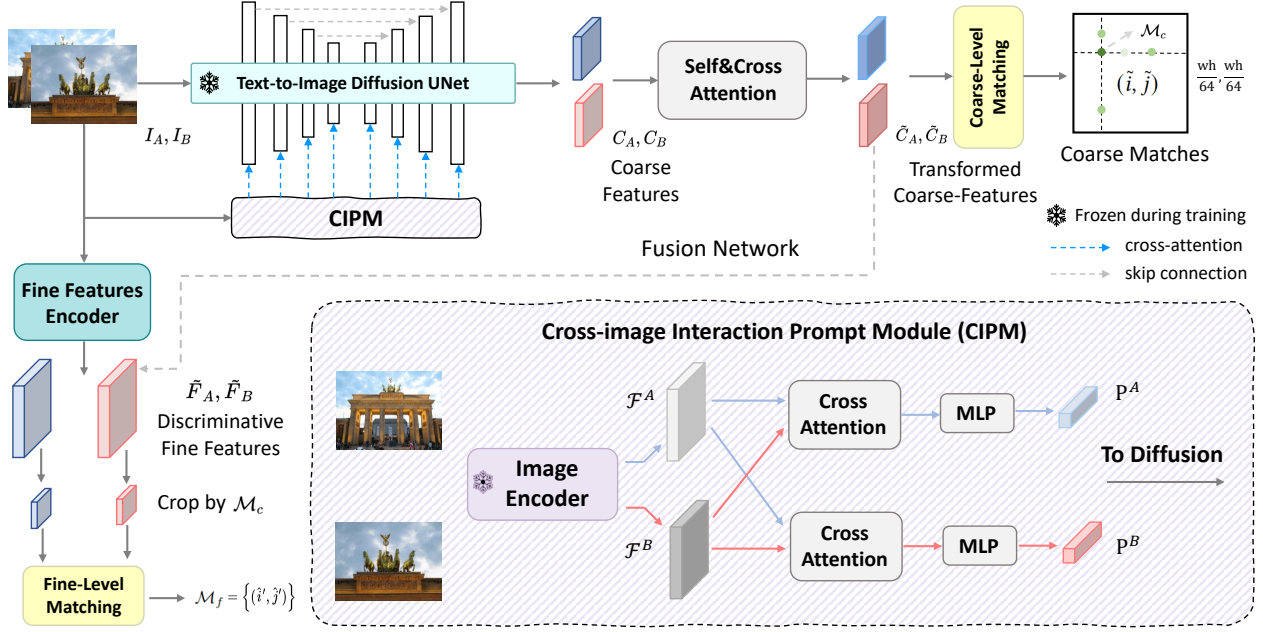


Figure 2. **Pipeline Overview.** Given an image pair, we first encode them with the image encoder and employ the cross-attention mechanism to proceed with explicit interaction between images. With the images and its prompt containing interactive information as input, we extract their coarse features C_A, C_B from a frozen text-to-image diffusion UNet. Then, we refine the coarse features for more discriminative by iteratively applying self- and cross-attention mechanisms. The coarse-level matching generates pixel-to-pixel matches \mathcal{M}_c at 1/8 scale. To refine coarse matches, discriminative fine features \tilde{F}_A, \tilde{F}_B are obtained by fusing the transformed coarse features with original fine features from the specialized fine feature encoder. Feature patches are then cropped, centered around each coarse match \mathcal{M}_c . The fine-level matching is followed to obtain sub-pixel matches \mathcal{M}_f .

dation models as feature extractor directly, significantly improving the performance. However, we identify that they ignored the critical misalignment between foundation models and the matching tasks. Specifically, the commonly used DINOv2 [34] often loses information about specific instances. Meanwhile these models lack information interaction between image pairs, leading to failures in multiple instances scenes. In contrast, we propose to integrating the generative-based diffusion models to address the misalignment with a novel cross-image interaction module, achieving excellent performance in multi-instance scenes.

Building on superior generative performance of diffusion models, recent studies have started investigating the internal representations within diffusion models [40, 57, 58, 62]. DIFT [51] and SD+DINO [59] demonstrated that extracting features from denoising module enables semantic matching between two objects. In addition, DIFT has also shown that the image features from frozen diffusion models can act as powerful descriptors for feature matching tasks. Our work is closely supported by these efforts, but we instead explore the misalignment when adapting the foundation models into feature matching and how to overcome.

Cross-image Interaction. Mainstream approaches such as RoMa [15] and OmniGlue [21] utilize visual foundation models to process individual images, thereby obtaining in-

dependent image features. The relationship between the images is obtained through a subsequent attention mechanism. However, we argue that performing matching using image features extracted in this way limited performance through the image features lacking correlation. CroCo [55] and CroCov2 [56] leverage cross-view completion as a pre-training objective to inherently encourage the model to learn correlated features cross images. SD4Match [23] has underscored the importance of the relevance of cross-image in semantic matching, which employ a shared prompt conditioned on the image pairs for diffusion model. Nevertheless, this work faces notable issue: this shared prompt introduces correlation while leading to worse discriminative. In contrast, our proposed CIPM provided the personalized prompts for each image, guiding feature extraction to increase relevance while maintaining discriminancy. Our IMD not only improves information transfer across images but also results in correlated features.

3. Method

In this section, we present IMD, a new detector-free local feature matching method to overcome the misalignment between vision foundation models and feature matching. IMD adopts a typical two-stage framework, starting with coarse-level correspondences and subsequently refining them to

sub-pixel positions. Given a pair of images I_A and I_B , the UNet component within diffusion models generates coarse feature maps (1/8) from input images based on the prompt produced by our designed prompting module (Sec. 3.2). Specifically, we propose the cross-image interaction prompt module to explicitly facilitate cross-image interaction. With these extracted features, the self- and cross-attention based coarse matching is performed in coarse-level features (Sec. 3.3). Using the specialized fine features encoder, we extract the fine feature maps (1/2) from image pairs. According to the coarse matches, a subpixel-level refinement module is employed to predict fine-level matches (Sec 3.4). An overview of our approach is illustrated in Figure 2.

3.1. Text-to-Image Diffusion Model

We begin with a brief overview of the diffusion model and its adaptation for feature extraction.

Background. Diffusion models [19, 20, 48] are generative models that are designed to transform a normal distribution to an arbitrary data distribution. This model involves two processes: forward and reverse. In the forward process, Gaussian noise of varying magnitudes is added to clean data points to create noisy data samples. A clean image I_0 is gradually degraded to a noisy image I_t through a series of Gaussian noise additions, following the equation:

$$I_t = \sqrt{\alpha_t}I_0 + (\sqrt{1 - \alpha_t})\epsilon, \quad (1)$$

where $\epsilon \sim \mathcal{N}(0, 1)$ denotes the randomly sampled noise, and $t \in [0, T]$ represents the “time” in the diffusion process with larger time steps corresponding to higher levels of noise. The noise amount is controlled by the pre-defined noise schedule $\{\alpha_t\}_t^T$. In the reverse process, a neural network f_θ is trained to take I_t and the time step t as inputs to predict the added noise ϵ . For image generation, f_θ is typically parametrized as a UNet [13, 38]. Once trained, f_θ can be utilized to “reverse” the diffusion process. Thus, by sampling from a normal distribution, the corresponding “original image” can be reconstructed through iterative removal of the noise ϵ .

Diffusion Model as Feature Extractor. Our framework is built upon the widely used Stable Diffusion (SD) [38] models, which perform the denoising process in a learned latent space using a UNet architecture. SD also exhibits impressive capability to generate high-quality images conditioned on input prompts, such as text or images. Given an input image I_0 and a specific timestep t , I_0 is first encoded into its latent representation z_0 using a VAE encoder \mathcal{E} , which is subsequently corrupted to z_t using Eq. (1). During this noise prediction process, with the latent code z_t at timestep t and the prompt embedding P as inputs, we extract the feature map F from the output of an intermediate layer of denoising UNet. This process can be formally expressed as

follows:

$$\begin{aligned} z_0 &= \mathcal{E}(I_0), \\ z_t &= \sqrt{\alpha_t}z_0 + \sqrt{1 - \alpha_t}\epsilon, \\ F &= \text{UNet}(z_t, t, P). \end{aligned} \quad (2)$$

Another important consideration is the selection of the timestep t and the network layer from which features are extracted. Studies indicate larger t and earlier network layers tend to produce more semantically-aware features, while smaller t and later layers emphasize low-level details [51]. For a detailed overview of the hyper-parameter values utilized in this study, please refer to the Suppl. For simplicity, we omit the VAE encoding step and directly refer to the input to the UNet as the image I rather than its latent representation z in the following sections.

3.2. Cross-image Interaction Prompt Module

Text-to-image diffusion models pre-trained on extensive image-text pair datasets, exhibit remarkable controllability through customizable prompt mechanisms. During each step of the denoising process, diffusion models perform cross-attention between the text embedding of prompts and UNet features leverage the text input to guide the denoising direction of the noisy image. As shown in Eq.(2), the diffusion model’s visual representation F of image I relies on its associated prompt P . This motivated us to explore the possibility of using another image as a prompt to generate interactive image features.

Recent studies have explored generating the prompts with input images for tasks such as semantic correspondence [23, 59] and image segmentation [57]. In this context, the prompt is generated from the input image itself in single-image task or a shared prompt by concatenating the features from the image pair in tasks involving a pair of images. Although this design has proven effective for the aforementioned tasks, it may be not the optimal choice for facilitating image interaction in feature matching. Our reasons are:

1. Feature matching requires the model to focus on the local features of the images. Utilizing a shared prompt for feature extraction across image pairs can result in the loss of detailed information from the images.
2. Simply concatenating image features is insufficient to fully capture the relationships between them, as it lacks explicit learning of dependencies and interactive information between the images.

We therefore propose a novel cross-image interaction prompt module (CIPM) and illustrate its architecture in the bottom of Figure 2. Given a pair of clean images I_A and I_B , we leverage a pre-trained frozen image encoder \mathcal{V} , e.g., from CLIP [36] to extract the image features \mathcal{F}^A and \mathcal{F}^B . Then we adopt three 1×1 convolution layers to encode the input image feature \mathcal{F}^A and \mathcal{F}^B into features $\phi_{Q,I}$,

$\phi_{K,I}, \phi_{V,I}$. We apply the cross-attention mechanism between features from input images I_A and I_B . We further utilize a learned MLP to transform the image embedding into the prompt embedding P_A and P_B , which is then fed into the text-to-image diffusion UNet, denoted as:

$$\begin{aligned} P_A &= \text{MLP} \circ \text{Softmax}(\phi_{Q,I_A} \phi_{K,I_B} / \sqrt{d_k}) \phi_{V,I_B}, \\ P_B &= \text{MLP} \circ \text{Softmax}(\phi_{Q,I_B} \phi_{K,I_A} / \sqrt{d_k}) \phi_{V,I_A}, \end{aligned} \quad (3)$$

where d_k denote the scale factor. Finally, the UNet of the text-to-image diffusion model, combined with the CIPM, constitutes IMD's feature extractor, which generates the visual representation for the given image pairs. Formally, the coarse features C_A and C_B are computed as:

$$\begin{aligned} C_A &= \text{UNet}(I_A, t, P_A), \\ C_B &= \text{UNet}(I_B, t, P_B). \end{aligned} \quad (4)$$

The attention mechanism facilitates interaction between the input images I_A and I_B within the feature space, thereby capturing correspondence information more explicitly compared to merely concatenating the image pair channel-wise before feeding them into the network [23]. Furthermore, the transformer-based network demonstrates greater robustness when the two input images have significant differences.

3.3. Coarse-Level Matching Module

We also conduct the attention mechanisms for coarse features to improve discriminativeness and compute coarse-level matches using the transformed coarse feature maps \tilde{C}_A and \tilde{C}_B . These coarse correspondences provide rough matching regions that are refined in the subsequent fine-level refinement module. The score matrix \mathcal{S} is generated by computing the pairwise cosine similarity between coarse-level features \tilde{C}_A and \tilde{C}_B . We also apply the dual-softmax of \mathcal{S} to obtain the probability of mutual nearest matching, following [8, 9, 49]. The coarse matches $\{\mathcal{M}_c\}$ are determined by selecting matches that exceed a predefined score threshold τ and satisfy the mutual nearest neighbor (MNN) constraint.

3.4. Subpixel-Level Refinement Module

As illustrated in Figure 2, with the established coarse matches $\{\mathcal{M}_c\}$, we refine these matches to achieve sub-pixel accuracy following [54]. This module consists of a specialized fine feature encoder for generating discriminative fine features, followed by the fine-level refinement to produce the final matches $\{\mathcal{M}_f\}$.

Fine Features Encoder. In prior works [9, 49], the FPN [26] is employed for producing a feature pyramid of coarse and fine features used for coarse matching and later refined to a sub-pixel level. This is problematic when using SD features as only coarse features at 1/8 dimension

of the original image exist. Hence, we utilize a specialized ConvNet obtained fine features at 1/2 dimension. For efficiency, these fine image features are fusion with the previously transformed coarse features to obtain discriminative fine features \tilde{F}_A, \tilde{F}_B in the original image resolution eliminating the additional transform networks [49]. Then local feature patches are cropped on fine feature maps centered at each coarse match $\{\mathcal{M}_c\}$.

Fine-Level Matching. To refine the coarse matches, we first compute the local patch score matrix \mathcal{S}_l with the fine feature patches. MNN searching is applied on \mathcal{S}_l to get intermediate pixel-level fine matches. We select the top-1 fine match for each coarse match by ranking the correlation scores. Then the feature of each point in I_A is correlated with a 3×3 feature patch centered around its fine match in I_B . The softmax operation is applied to obtain a match distribution matrix, and the final refined match is determined by calculating the expectation.

3.5. Supervision

The entire pipeline is trained in an end-to-end manner, with separate supervision applied to the coarse and refinement matching modules.

Coarse-Level Matching Supervision. The coarse-level loss is computed as the focal loss between the matching score matrix and the ground truth matches. The coarse ground truth matches, denoted as $\{\mathcal{M}_c\}_{gt}$, with a total number of N , are constructed by warping grid-level points from I_A to I_B using depth maps and image poses following [49]. The resulting correlation score matrix \mathcal{S} in coarse matching is supervised by minimizing the log-likelihood loss over the locations in $\{\mathcal{M}_c\}_{gt}$:

$$\mathcal{L}_c = -\frac{1}{N} \sum_{(\tilde{i}, \tilde{j}) \in \{\mathcal{M}_c\}_{gt}} \log \mathcal{S}(\tilde{i}, \tilde{j}). \quad (5)$$

Fine-Level Matching Supervision. We train the fine-level matching module by supervising two losses independently. The first fine loss, \mathcal{L}_{f1} , aims to minimize the log-likelihood loss of each fine local score matrix \mathcal{S}_l based on the pixel-level ground truth fine matches, similar to the coarse loss. The second is optimized using \mathcal{L}_{f2} , which computes the ℓ_2 loss between the final subpixel matches $\{\mathcal{M}_f\}$ and the ground truth fine matches $\{\mathcal{M}_f\}_{gt}$.

The total loss is computed as a weighted sum of all supervision terms: $\mathcal{L} = \mathcal{L}_c + \alpha \mathcal{L}_{f1} + \beta \mathcal{L}_{f2}$.

4. Experiments

4.1. Implementation Details

Following DIFT [51], we employ Stable Diffusion (SD) 2-1 [38] pretrained on LAION [47] dataset as the diffusion

Table 1. **Results of multi-instance evaluation on IMIM and two-view pose estimation on the MegaDepth [24], ScanNet [11] datasets.** Methods are grouped into 3 groups: 1) methods that are zero-shot and not fine-tuned on the training data, 2) sparse methods, and 3) semi-dense methods. All the IMD results have gray background for easy lookup and annotate **best** results. The extended version including dense methods, is provided in the Suppl.

Category	Method	MegaDepth			ScanNet			IMIM (%)
		AUC@5°	AUC@10°	AUC@20°	AUC@5°	AUC@10°	AUC@20°	
Zero-Shot	CLIP [36] <small>ICML'21</small>	30.8	48.1	63.2	10.1	20.6	31.3	54.4
	DINOv2 [34] <small>Arxiv'23</small>	32.5	50.8	65.3	13.0	28.5	40.8	57.9
	DIFT [51] <small>NeurIPS'23</small>	38.4	55.9	70.5	15.7	32.0	45.1	61.2
Sparse	SP [12]+NN <small>CVPRW'23</small>	31.7	46.8	60.1	7.5	18.6	32.1	55.9
	OmniGlue [21] <small>CVPR'24</small>	47.4	65.0	77.8	31.3	50.2	65.0	77.6
	SP [12]+LG [27] <small>ICCV'23</small>	49.9	67.0	80.1	14.8	30.8	47.5	60.5
Semi-Dense	LoFTR [49] <small>CVPR'21</small>	52.8	69.2	81.2	16.9	33.6	50.6	68.9
	RCM [31] <small>ECCV'24</small>	53.2	69.4	81.5	17.3	34.6	52.1	-
	Efficient LoFTR [54] <small>CVPR'24</small>	56.4	72.2	83.5	19.2	37.0	53.6	70.6
	EcoMatcher [10] <small>ECCV'24</small>	56.5	72.0	83.4	-	-	-	-
	HomoMatcher [53] <small>AAAI'25</small>	57.8	73.5	84.4	22.1	40.9	57.5	-
	TopicFM [16] <small>AAAI'23</small>	58.2	72.8	83.2	17.3	34.5	50.9	76.5
	MESA_ASpan [61] <small>CVPR'24</small>	58.4	74.1	84.8	-	-	-	-
	CasMTR [8] <small>ICCV'23</small>	59.1	74.3	84.8	22.6	40.7	58.0	79.2
	PRISM [7] <small>ACMMM'24</small>	60.0	74.9	85.1	23.9	41.8	58.9	-
	IMD (Ours)	61.2	76.0	85.8	29.8	48.3	64.2	88.7

model. We utilize the upsampling block index $n = 2$ of the UNet so the feature map size is 1/8 of the input and the dimension is 640, and we set the time step used for the diffusion process to $t = 0$. We choose CLIP [36] as the image encoder \mathcal{V} in CIPM. We adopt the ResNet [17] to extract fine image features. The self- and cross-attention are interleaved for $N = 2$ times to transform coarse features. τ is chosen to 0.2. Our model is trained on the MegaDepth dataset [24], a large-scale outdoor dataset. Following the protocol in [54], the test scenes are strictly separated from the training data. The weights α and β in the loss function are set to 1.0 and 0.25, respectively. We employ the AdamW optimizer with an initial learning rate of 4×10^{-3} . The training process takes 30 epochs on 8 NVIDIA 3090 GPUs. Both the coarse and fine stages are trained jointly from scratch. The model trained on MegaDepth is subsequently evaluated across all datasets to showcase its generalization capability.

4.2. Evaluation Dataset for Multi-Instances

Datasets. During the evaluation of IMD on conventional datasets for matching tasks, we observed that most existing datasets primarily have only a single instance per object category. For example, widely used benchmarks like MegaDepth [24] and ScanNet [11] focus on individual landmarks such as buildings, with each category typically representing only one instance. These characteristics make it easier for global semantic-based methods to get accurate matching results, as there are often no objects from the same category but different instances need to distinguish within

or across images. As a result, comparing instance-based features against current methods on these benchmarks tends to yield similar results, which does not fully showcase the advantages of instance-based approaches.

To this end, we propose a new benchmark: Image Multi-Instance Matching (IMIM). IMIM is built using the BURST [1] dataset designed for Segmentation and Tracking inspired by [40]. This dataset consists of videos with pixel-level segmentation masks for each unique object track across different object categories. Specifically, we select videos that include at least two instances of the same object class and pick two frames from videos every time, assigning one as the source image and another used for the target image. After filtering, we obtain a total of 100 pairs images from 50 videos across 10 object categories.

Evaluation Protocol. Ground-truth masks are used to crop instances from source and target images. For every match results (i, j) , we calculate the number N of matching pairs that satisfied i located in the source image instance mask. We report the percentage of M/N that M is the number of matching pairs which satisfied i located in the source image instance mask, while j located in the target image instance mask.

Results. Table 1 presents the results in IMIM. IMD demonstrates superior performance over methods designed specifically for matching task and zero-shot models including CLIP, DINOv2, DIFT with diffusion, demonstrating our approach’s reliable ability when matching the multi instances in the target image. Notably, we observe significant discrep-

Table 2. **Results of Homography Estimation on Hpatches Dataset.**

Category	Method	Homography est. AUC		
		@3px	@5px	10px
Sparse	R2D2 [37]+NN <small>NeurIPS'19</small>	50.6	63.9	76.8
	OmniGlue [21] <small>CVPR'24</small>	55.3	69.0	82.5
	SP [12]+SG [42] <small>CVPR'20</small>	53.9	68.3	81.7
	LoFTR [49] <small>CVPR'21</small>	65.9	75.6	84.6
Semi-Dense	Efficient LoFTR [54] <small>CVPR'24</small>	66.5	76.4	85.5
	HomoMatcher [53] <small>AAAI'25</small>	70.2	79.6	87.8
	SRMatcher [28] <small>ACMMM'24</small>	71.2	79.3	87.0
	CasMTR [8] <small>ICCV'23</small>	71.4	80.2	87.9
	PRISM [7] <small>ACMMM'24</small>	71.9	80.4	88.3
	IMD (Ours)	73.9	82.0	88.9

ancies between DINOv2 and DIFT. This due to DINOv2 ignoring the information not related to semantics. Qualitative comparisons are shown in Figure 3, demonstrating that our approach consistently and accurately matches the correct instance in the target image. Our experimental results validate the effectiveness of the proposed approach in significantly mitigating the misalignment issue.

4.3. Relative Pose Estimation

Datasets. We utilize the outdoor MegaDepth [24] dataset and the indoor ScanNet [11] dataset to evaluate relative pose estimation, showcasing the effectiveness of our approach.

MegaDepth is an extensive outdoor dataset comprising 1 million images across 196 scenes, reconstructed using COLMAP [45]. The key challenges in this dataset include significant viewpoint and illumination variations, along with repetitive patterns. For evaluation, we adopt the test split from [49], using 1500 sampled pairs from the "Sacré Coeur" and "St. Peter's Square" scenes. All images are resized such that the longest edge equals 1152 pixels.

ScanNet consists of monocular sequences with ground truth annotations and presents challenges due to wide baselines and textureless regions. For evaluation, we use the test pairs sampled in [49], resizing all images to 640×480 pixels for all methods.

Evaluation Protocol. Following [49, 54], the recovered relative poses from the matches are evaluated to assess matching accuracy. The pose error is defined as the maximum of the angular errors in rotation and translation. We evaluate the performance by reporting the AUC of pose error at thresholds of 5° , 10° , and 20° .

Results. We report the accuracy comparison between IMD and other methods in Table 1. Qualitative comparisons are shown in Figure 3. Our proposed IMD sets a new state-of-the-art performance across all evaluation metrics on outdoor benchmarks. Benefiting from the use of pre-trained diffusion backbone, IMD notably improves by 24.6% in AUC@ 5° on ScanNet compared to the best model trained on MegaDepth PRISM, showing impressive generalization capability. We have the extended version of quantitative re-

Table 3. **Results of Visual Localization on InLoc Dataset.**

Method	DUC1	DUC2
	(0.25m, 2°)/(0.5m, 5°)/(1.0m, 10°)	
SP [12]+SG [42] <small>CVPR'20</small>	49.0 / 68.7 / 80.8	53.4 / 77.1 / 82.4
LoFTR [49] <small>CVPR'21</small>	47.5 / 72.2 / 84.8	54.2 / 74.8 / 85.5
CasMTR [8] <small>ICCV'23</small>	53.5 / 76.8 / 85.4	51.9 / 70.2 / 83.2
AspanFormer [9] <small>ECCV'22</small>	51.5 / 73.7 / 86.0	55.0 / 74.0 / 81.7
PRISM [7] <small>ACMMM'24</small>	53.0 / 77.8 / 87.9	54.2 / 72.5 / 83.2
IMD (Ours)	54.6 / 77.3 / 88.2	60.3 / 82.7 / 88.5

sults (e.g. dense methods) and more analysis in the Suppl.

4.4. Homography Estimation

Dataset. Homography is crucial in two-view geometry, facilitating the transformation of perspectives between two images capturing the same scene. We evaluate on the widely used HPatches dataset [2], which includes 57 sequences with significant illumination variations and 59 sequences exhibiting significant viewpoint changes.

Evaluation Protocol. We present the area under the cumulative curve (AUC) for corner errors at thresholds of 3, 5, and 10 pixels. OpenCV's RANSAC method is used for robust estimation. Following LoFTR [49], all test images are resized so that their shorter dimension equals 480 pixels.

Results. Table 2 demonstrates that IMD significantly outperforms sparse and semi-dense methods. For the semi-dense methods, our method notably improves by 2.7% in @3px compared to the best semi-dense methods. We attribute this to the effectiveness of guidance from the diffusion model for generalization and the proposed image interaction module for accuracy improvement.

4.5. Visual Localization

Datasets and Evaluation Protocols. We evaluate the performance of IMD on the widely-used datasets InLoc [50]. The InLoc dataset includes 9,972 RGBD images with geometric registration and 329 query images with verified poses, posing challenges in textureless or repetitive environments. For testing, we focus on DUC1 and DUC2 following [49]. The candidate image pairs are identified using the pre-trained HLoc [41] system following [7]. The results of Aachen Day-Night v1.1 [44] are provided in Suppl.

Results. Table 3 presents the result on the InLoc dataset, IMD surpasses all methods on DUC2 and matches the performance of top-tier approaches on DUC1. IMD exhibits robust performances, underscoring the adaptability of our method in diverse task environments.

4.6. Ablation Studies

Visual Representations. We compare the internal representations of diffusion models with those of other pre-trained contrastive learning objective and discriminative objective models. We observe that IMD outperforms the other

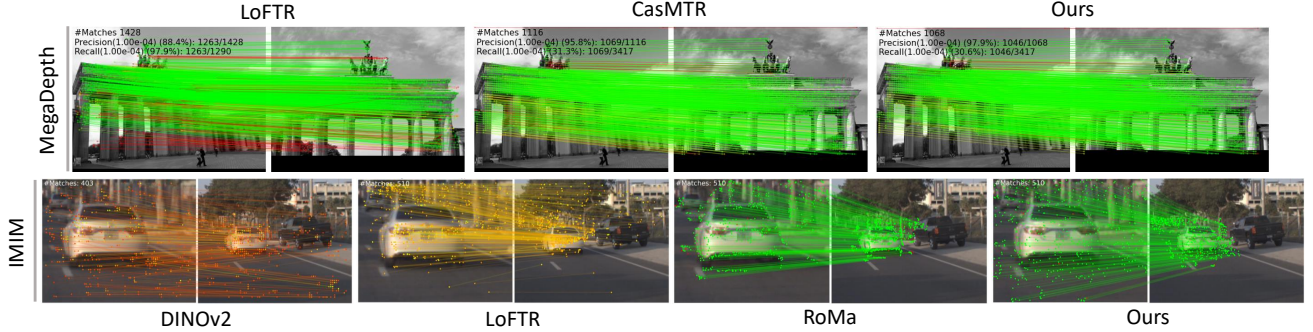


Figure 3. **Qualitative comparison** of outdoor MegaDepth and IMIM datasets compared with DINOv2 [34], LoFTR [49], CasMTR [8], RoMa [15] and ours IMD. Green indicates the correctly matching results. More visualizations are provided in the Suppl.

Table 4. **Results of Ablation Studies.**

Method	MegaDepth dataset			IMIM
	AUC@5°	AUC@10°	ACU@20°	
1) Replace SD to Swin (B) [29]	57.5	73.2	83.6	74.0
2) Replace SD to DINOv2 (B) [18]	57.8	73.5	83.7	75.5
3) Empty string	58.4	73.8	84.1	84.0
4) Individual prompt in CIPM	59.6	74.3	84.5	85.2
5) w/o cross attention	60.7	75.0	85.1	87.4
6) time step T = 100	60.9	75.7	85.8	88.1
Ours Full	61.2	76.0	85.8	88.7

models on both datasets. This highlights that internal representations of diffusion models are indeed more efficient for matching tasks, especially in multi-instance scenarios. More comparison results shown in Suppl.

Cross-image Interaction Prompt Module. We explore the influence of interaction in CIPM on matching accuracy. Specifically, we assess the additional approaches: an empty string and the individual image prompt in Table 4. These evaluations are regarded as does not presuppose any information interaction. These setups yield lower accuracy, further highlighting the benefits of the interaction between image pairs, and facilitates more precise capturing of cross-image relationships. When we replace the cross-attention with a concatenation operation to execute interaction between images which means both images share the same prompt, there is a decline in performance in row 5.

Different Time Steps. We also investigate which diffusion step(s) are most effective for feature extraction. As the value of t increases, the amount of noise distortion added to the input image also increases. In Stable Diffusion [38], there are a total of 1000 time steps. From the row 6 of Table 4, we observe that all metrics decrease as t increases, with the best results achieved at $t = 0$ (ours). We conduct more ablation studies about timesteps and block-index in Suppl.

4.7. Understanding IMD

To mitigate potential bias, that the improvement of the model mostly achieved from increased parameters in SD 2-1 (1,300M), we compare with different backbone: (1) DI-

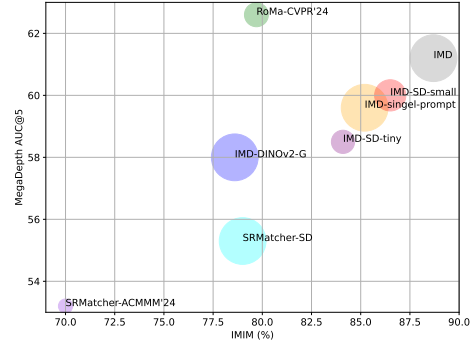


Figure 4. **Performance comparison** and the circle size indicating parameter count.

NOv2(G) (1,100M) of similar scale; (2) SD-tiny and SD-small with CIPM, having 75% and 55% fewer parameters respectively. We further compare with RoMa [15] (dense) and SRMatcher [28] (semi-dense) using DINOv2 and its SD 2-1 variant. Figure 4 shows results on MegaDepth and IMIM. All SD-based models achieve strong IMIM performance, indicating capacity alone does not address multi-instance problems. IMD-single-prompt results validate cross-image interaction effectiveness. Discussion on feature behavior analysis and training protocol ablations are detailed in Suppl.

5. Conclusion

In this work, we present IMD, a novel framework designed to address the misalignment between vision foundation models and feature matching tasks. We identify two challenges for addressing the misalignment: 1) foundation model properties' impact on matching; 2) the disconnect between foundation models and feature matching. We also introduce a new benchmark specifically designed to assess misalignment mitigation. Extensive experiments show that IMD achieves major gains and effectively alleviates misalignment. We expect our work will inspire future research on how to better utilize vision foundation models for downstream tasks, while also contributing to the broader utilization of these foundational models across diverse tasks.

6. Acknowledgment

This work was supported in part by the National Natural Science Foundation of China under Grants 62088102 and National Science and Technology Major Project (No. 2023ZD0121300).

References

- [1] Ali Athar, Jonathon Luiten, Paul Voigtlaender, Tarasha Khurana, Achal Dave, Bastian Leibe, and Deva Ramanan. Burst: A benchmark for unifying object recognition, segmentation and tracking in video. In *Proceedings of the IEEE/CVF winter conference on applications of computer vision*, pages 1674–1683, 2023. 2, 6
- [2] Vassileios Balntas, Karel Lenc, Andrea Vedaldi, and Krystian Mikolajczyk. Hpatches: A benchmark and evaluation of handcrafted and learned local descriptors. In *Proceedings of the IEEE conference on computer vision and pattern recognition*, pages 5173–5182, 2017. 7
- [3] Axel Barroso-Laguna, Edgar Riba, Daniel Ponsa, and Krystian Mikolajczyk. Key. net: Keypoint detection by handcrafted and learned cnn filters. In *Proceedings of the IEEE/CVF international conference on computer vision*, pages 5836–5844, 2019. 2
- [4] Herbert Bay, Tinne Tuytelaars, and Luc Van Gool. Surf: Speeded up robust features. In *Computer Vision—ECCV 2006: 9th European Conference on Computer Vision, Graz, Austria, May 7–13, 2006. Proceedings, Part I* 9, pages 404–417. Springer, 2006. 1
- [5] Herbert Bay, Andreas Ess, Tinne Tuytelaars, and Luc Van Gool. Speeded-up robust features (surf). *Computer vision and image understanding*, 110(3):346–359, 2008. 2
- [6] Xudong Cai, Yongcai Wang, Zhe Huang, Yu Shao, and Deying Li. Voloc: Visual place recognition by querying compressed lidar map. *arXiv preprint arXiv:2402.15961*, 2024. 1
- [7] Xudong Cai, Yongcai Wang, Lun Luo, Minhang Wang, Deying Li, Jintao Xu, Weihao Gu, and Rui Ai. Prism: Progressive dependency maximization for scale-invariant image matching. In *Proceedings of the 32nd ACM International Conference on Multimedia*, pages 5250–5259, 2024. 6, 7
- [8] Chenjie Cao and Yanwei Fu. Improving transformer-based image matching by cascaded capturing spatially informative keypoints. In *Proceedings of the IEEE/CVF International Conference on Computer Vision*, pages 12129–12139, 2023. 1, 2, 5, 6, 7, 8
- [9] Hongkai Chen, Zixin Luo, Lei Zhou, Yurun Tian, Mingmin Zhen, Tian Fang, David Mckinnon, Yanghai Tsin, and Long Quan. Aspanformer: Detector-free image matching with adaptive span transformer. In *European Conference on Computer Vision*, pages 20–36. Springer, 2022. 2, 5, 7
- [10] Peiqi Chen, Lei Yu, Yi Wan, Yongjun Zhang, Jian Wang, Liheng Zhong, Jingdong Chen, and Ming Yang. Ecomatcher: Efficient clustering oriented matcher for detector-free image matching. In *European Conference on Computer Vision*, pages 344–360. Springer, 2024. 6
- [11] Angela Dai, Angel X Chang, Manolis Savva, Maciej Halber, Thomas Funkhouser, and Matthias Nießner. Scannet: Richly-annotated 3d reconstructions of indoor scenes. In *Proceedings of the IEEE conference on computer vision and pattern recognition*, pages 5828–5839, 2017. 1, 6, 7
- [12] Daniel DeTone, Tomasz Malisiewicz, and Andrew Rabinovich. Superpoint: Self-supervised interest point detection and description. In *Proceedings of the IEEE conference on computer vision and pattern recognition workshops*, pages 224–236, 2018. 1, 2, 6, 7
- [13] Prafulla Dhariwal and Alexander Nichol. Diffusion models beat gans on image synthesis. *Advances in neural information processing systems*, 34:8780–8794, 2021. 4
- [14] Johan Edstedt, Ioannis Athanasiadis, Mårten Wadenbäck, and Michael Felsberg. Dkm: Dense kernelized feature matching for geometry estimation. In *Proceedings of the IEEE/CVF Conference on Computer Vision and Pattern Recognition*, pages 17765–17775, 2023. 1, 2
- [15] Johan Edstedt, Qiyu Sun, Georg Bökman, Mårten Wadenbäck, and Michael Felsberg. Roma: Robust dense feature matching. In *Proceedings of the IEEE/CVF Conference on Computer Vision and Pattern Recognition*, pages 19790–19800, 2024. 1, 2, 3, 8
- [16] Khang Truong Giang, Soohwan Song, and Sungho Jo. Topicfm: Robust and interpretable topic-assisted feature matching. In *Proceedings of the AAAI conference on artificial intelligence*, pages 2447–2455, 2023. 6
- [17] Kaiming He, Xiangyu Zhang, Shaoqing Ren, and Jian Sun. Deep residual learning for image recognition. In *Proceedings of the IEEE conference on computer vision and pattern recognition*, pages 770–778, 2016. 6
- [18] Kaiming He, Xinlei Chen, Saining Xie, Yanghao Li, Piotr Dollár, and Ross Girshick. Masked autoencoders are scalable vision learners. In *Proceedings of the IEEE/CVF conference on computer vision and pattern recognition*, pages 16000–16009, 2022. 8
- [19] Jonathan Ho, Ajay Jain, and Pieter Abbeel. Denoising diffusion probabilistic models. *Advances in neural information processing systems*, 33:6840–6851, 2020. 4
- [20] Xirui Hu, Jiahao Wang, Hao Chen, Weizhan Zhang, Benqi Wang, Yikun Li, and Haishun Nan. Dynamicid: Zero-shot multi-id image personalization with flexible facial editability. 2025. 4
- [21] Hanwen Jiang, Arjun Karpur, Bingyi Cao, Qixing Huang, and André Araujo. Omniglue: Generalizable feature matching with foundation model guidance. In *Proceedings of the IEEE/CVF Conference on Computer Vision and Pattern Recognition*, pages 19865–19875, 2024. 1, 2, 3, 6, 7
- [22] Alexander Kirillov, Eric Mintun, Nikhila Ravi, Hanzi Mao, Chloe Rolland, Laura Gustafson, Tete Xiao, Spencer Whitehead, Alexander C Berg, Wan-Yen Lo, et al. Segment anything. In *Proceedings of the IEEE/CVF international conference on computer vision*, pages 4015–4026, 2023. 2
- [23] Xinghui Li, Jingyi Lu, Kai Han, and Victor Adrian Prisacariu. Sd4match: Learning to prompt stable diffusion model for semantic matching. In *Proceedings of the IEEE/CVF Conference on Computer Vision and Pattern Recognition*, pages 27558–27568, 2024. 3, 4, 5

- [24] Zhengqi Li and Noah Snavely. Megadepth: Learning single-view depth prediction from internet photos. In *Proceedings of the IEEE conference on computer vision and pattern recognition*, pages 2041–2050, 2018. 1, 6, 7
- [25] Kang Liao, Lang Nie, Chunyu Lin, Zishuo Zheng, and Yao Zhao. Recretnet: Rectangling rectified wide-angle images by thin-plate spline model and dof-based curriculum learning. In *Proceedings of the IEEE/CVF International Conference on Computer Vision*, pages 10800–10809, 2023. 1
- [26] Tsung-Yi Lin, Piotr Dollár, Ross Girshick, Kaiming He, Bharath Hariharan, and Serge Belongie. Feature pyramid networks for object detection. In *Proceedings of the IEEE conference on computer vision and pattern recognition*, pages 2117–2125, 2017. 5
- [27] Philipp Lindenberger, Paul-Edouard Sarlin, and Marc Pollefeys. Lightglue: Local feature matching at light speed. In *Proceedings of the IEEE/CVF International Conference on Computer Vision*, pages 17627–17638, 2023. 1, 6
- [28] Yuhan Liu, Qianxin Huang, Siqi Hui, Jingwen Fu, Sanping Zhou, Kangyi Wu, Pengna Li, and Jinjun Wang. Semantic-aware representation learning for homography estimation. In *Proceedings of the 32nd ACM International Conference on Multimedia*, pages 2506–2514, 2024. 1, 2, 7, 8
- [29] Ze Liu, Yutong Lin, Yue Cao, Han Hu, Yixuan Wei, Zheng Zhang, Stephen Lin, and Baining Guo. Swin transformer: Hierarchical vision transformer using shifted windows. In *Proceedings of the IEEE/CVF international conference on computer vision*, pages 10012–10022, 2021. 8
- [30] David G Lowe. Distinctive image features from scale-invariant keypoints. *International journal of computer vision*, 60:91–110, 2004. 2
- [31] Xiaoyong Lu and Songlin Du. Raising the ceiling: Conflict-free local feature matching with dynamic view switching. In *European Conference on Computer Vision*, pages 256–273. Springer, 2024. 6
- [32] Jisu Nam, Gyuseong Lee, Sunwoo Kim, Hyeonsu Kim, Hyoungwon Cho, Seyeon Kim, and Seungryong Kim. Diffusion model for dense matching. *arXiv preprint arXiv:2305.19094*, 2023. 2
- [33] Lang Nie, Chunyu Lin, Kang Liao, Shuaicheng Liu, and Yao Zhao. Unsupervised deep image stitching: Reconstructing stitched features to images. *IEEE Transactions on Image Processing*, 30:6184–6197, 2021. 1
- [34] Maxime Oquab, Timothée Darcet, Théo Moutakanni, Huy Vo, Marc Szafraniec, Vasil Khalidov, Pierre Fernandez, Daniel Haziza, Francisco Massa, Alaaeldin El-Nouby, et al. Dinov2: Learning robust visual features without supervision. *arXiv preprint arXiv:2304.07193*, 2023. 3, 6, 8
- [35] Guilherme Potje, Felipe Cadar, André Araujo, Renato Martins, and Erickson R Nascimento. Enhancing deformable local features by jointly learning to detect and describe keypoints. In *Proceedings of the IEEE/CVF Conference on Computer Vision and Pattern Recognition*, pages 1306–1315, 2023. 1
- [36] Alec Radford, Jong Wook Kim, Chris Hallacy, Aditya Ramesh, Gabriel Goh, Sandhini Agarwal, Girish Sastry, Amanda Askell, Pamela Mishkin, Jack Clark, et al. Learning transferable visual models from natural language supervision. In *International conference on machine learning*, pages 8748–8763. PMLR, 2021. 4, 6
- [37] Jerome Revaud, Cesar De Souza, Martin Humenberger, and Philippe Weinzaepfel. R2d2: Reliable and repeatable detector and descriptor. *Advances in neural information processing systems*, 32, 2019. 1, 7
- [38] Robin Rombach, Andreas Blattmann, Dominik Lorenz, Patrick Esser, and Björn Ommer. High-resolution image synthesis with latent diffusion models. In *Proceedings of the IEEE/CVF conference on computer vision and pattern recognition*, pages 10684–10695, 2022. 4, 5, 8
- [39] Ethan Rublee, Vincent Rabaud, Kurt Konolige, and Gary Bradski. Orb: An efficient alternative to sift or surf. In *2011 International conference on computer vision*, pages 2564–2571. Ieee, 2011. 1, 2
- [40] Dvir Samuel, Rami Ben-Ari, Matan Levy, Nir Darshan, and Gal Chechik. Where’s waldo: Diffusion features for personalized segmentation and retrieval. In *The Thirty-eighth Annual Conference on Neural Information Processing Systems*, 2024. 2, 3, 6
- [41] Paul-Edouard Sarlin, Cesar Cadena, Roland Siegwart, and Marcin Dymczyk. From coarse to fine: Robust hierarchical localization at large scale. In *Proceedings of the IEEE/CVF conference on computer vision and pattern recognition*, pages 12716–12725, 2019. 1, 7
- [42] Paul-Edouard Sarlin, Daniel DeTone, Tomasz Malisiewicz, and Andrew Rabinovich. Superglue: Learning feature matching with graph neural networks. In *Proceedings of the IEEE/CVF conference on computer vision and pattern recognition*, pages 4938–4947, 2020. 2, 7
- [43] Paul-Edouard Sarlin, Ajaykumar Unagar, Mans Larsson, Hugo Germain, Carl Toft, Viktor Larsson, Marc Pollefeys, Vincent Lepetit, Lars Hammarstrand, Fredrik Kahl, et al. Back to the feature: Learning robust camera localization from pixels to pose. In *Proceedings of the IEEE/CVF conference on computer vision and pattern recognition*, pages 3247–3257, 2021. 1
- [44] Torsten Sattler, Will Maddern, Carl Toft, Akihiko Torii, Lars Hammarstrand, Erik Stenborg, Daniel Safari, Masatoshi Okutomi, Marc Pollefeys, Josef Sivic, et al. Benchmarking 6dof outdoor visual localization in changing conditions. In *Proceedings of the IEEE conference on computer vision and pattern recognition*, pages 8601–8610, 2018. 7
- [45] Johannes L Schonberger and Jan-Michael Frahm. Structure-from-motion revisited. In *Proceedings of the IEEE conference on computer vision and pattern recognition*, pages 4104–4113, 2016. 1, 7
- [46] Johannes L Schönberger, Enliang Zheng, Jan-Michael Frahm, and Marc Pollefeys. Pixelwise view selection for unstructured multi-view stereo. In *Computer Vision—ECCV 2016: 14th European Conference, Amsterdam, The Netherlands, October 11–14, 2016, Proceedings, Part III 14*, pages 501–518. Springer, 2016. 1
- [47] Christoph Schuhmann, Romain Beaumont, Richard Vencu, Cade Gordon, Ross Wightman, Mehdi Cherti, Theo Coombes, Aarush Katta, Clayton Mullis, Mitchell Wortsman, et al. Laion-5b: An open large-scale dataset for training

- next generation image-text models. *Advances in Neural Information Processing Systems*, 35:25278–25294, 2022. 5
- [48] Jiaming Song, Chenlin Meng, and Stefano Ermon. Denoising diffusion implicit models. *arXiv preprint arXiv:2010.02502*, 2020. 4
- [49] Jiaming Sun, Zehong Shen, Yuang Wang, Hujun Bao, and Xiaowei Zhou. Loftr: Detector-free local feature matching with transformers. In *Proceedings of the IEEE/CVF conference on computer vision and pattern recognition*, pages 8922–8931, 2021. 1, 2, 5, 6, 7, 8
- [50] Hajime Taira, Masatoshi Okutomi, Torsten Sattler, Mircea Cimpoi, Marc Pollefeys, Josef Sivic, Tomas Pajdla, and Akihiko Torii. Inloc: Indoor visual localization with dense matching and view synthesis. In *Proceedings of the IEEE Conference on Computer Vision and Pattern Recognition*, pages 7199–7209, 2018. 7
- [51] Luming Tang, Menglin Jia, Qianqian Wang, Cheng Perng Phoo, and Bharath Hariharan. Emergent correspondence from image diffusion. *Advances in Neural Information Processing Systems*, 36:1363–1389, 2023. 2, 3, 4, 5, 6
- [52] Shitao Tang, Jiahui Zhang, Siyu Zhu, and Ping Tan. Quadtree attention for vision transformers. *arXiv preprint arXiv:2201.02767*, 2022. 1, 2
- [53] Xiaolong Wang, Lei Yu, Yingying Zhang, Jiangwei Lao, Lixiang Ru, Liheng Zhong, Jingdong Chen, Yu Zhang, and Ming Yang. Homomatcher: Dense feature matching results with semi-dense efficiency by homography estimation. *arXiv preprint arXiv:2411.06700*, 2024. 6, 7
- [54] Yifan Wang, Xingyi He, Sida Peng, Dongli Tan, and Xiaowei Zhou. Efficient loftr: Semi-dense local feature matching with sparse-like speed. In *Proceedings of the IEEE/CVF Conference on Computer Vision and Pattern Recognition*, pages 21666–21675, 2024. 5, 6, 7
- [55] Philippe Weinzaepfel, Vincent Leroy, Thomas Lucas, Romain Brégier, Yohann Cabon, Vaibhav Arora, Leonid Antsfeld, Boris Chidlovskii, Gabriela Csurka, and Jérôme Revaud. Croco: Self-supervised pre-training for 3d vision tasks by cross-view completion. *Advances in Neural Information Processing Systems*, 35:3502–3516, 2022. 3
- [56] Philippe Weinzaepfel, Thomas Lucas, Vincent Leroy, Yohann Cabon, Vaibhav Arora, Romain Brégier, Gabriela Csurka, Leonid Antsfeld, Boris Chidlovskii, and Jérôme Revaud. Croco v2: Improved cross-view completion pre-training for stereo matching and optical flow. In *Proceedings of the IEEE/CVF International Conference on Computer Vision*, pages 17969–17980, 2023. 3
- [57] Jiarui Xu, Sifei Liu, Arash Vahdat, Wonmin Byeon, Xiaolong Wang, and Shalini De Mello. Open-vocabulary panoptic segmentation with text-to-image diffusion models. In *Proceedings of the IEEE/CVF Conference on Computer Vision and Pattern Recognition*, pages 2955–2966, 2023. 3, 4
- [58] Junyi Zhang, Charles Herrmann, Junhwa Hur, Eric Chen, Varun Jampani, Deqing Sun, and Ming-Hsuan Yang. Telling left from right: Identifying geometry-aware semantic correspondence. In *Proceedings of the IEEE/CVF Conference on Computer Vision and Pattern Recognition*, pages 3076–3085, 2024. 3
- [59] Junyi Zhang, Charles Herrmann, Junhwa Hur, Luisa Polania Cabrera, Varun Jampani, Deqing Sun, and Ming-Hsuan Yang. A tale of two features: Stable diffusion complements dino for zero-shot semantic correspondence. *Advances in Neural Information Processing Systems*, 36, 2024. 2, 3, 4
- [60] Shihua Zhang and Jiayi Ma. Diffglue: Diffusion-aided image feature matching. In *Proceedings of the 32nd ACM International Conference on Multimedia*, pages 8451–8460, 2024. 2
- [61] Yesheng Zhang and Xu Zhao. Mesa: Matching everything by segmenting anything. In *Proceedings of the IEEE/CVF Conference on Computer Vision and Pattern Recognition*, pages 20217–20226, 2024. 2, 6
- [62] Wenliang Zhao, Yongming Rao, Zuyan Liu, Benlin Liu, Jie Zhou, and Jiwen Lu. Unleashing text-to-image diffusion models for visual perception. In *Proceedings of the IEEE/CVF International Conference on Computer Vision*, pages 5729–5739, 2023. 3
- [63] Shengjie Zhu and Xiaoming Liu. Pmatch: Paired masked image modeling for dense geometric matching. In *Proceedings of the IEEE/CVF Conference on Computer Vision and Pattern Recognition*, pages 21909–21918, 2023. 2